Dislocation arrangements in pentacene thin films

B. Nickel,[1,2,*] R. Barabash,[3,†] R. Ruiz,[4,‡] N. Koch,[2,5] A. Kahn,[5] L. C. Feldman,[4] R. F. Haglund,[4] and G. Scoles[1,2]
[1]*Chemistry Department, Princeton University, Princeton, New Jersey 08544, USA*
[2]*Princeton Materials Institute, Princeton, New Jersey 08544, USA*
[3]*Oak Ridge National Laboratory, Metals and Ceramics Division, Oak Ridge, Tennessee 37831-6188, USA*
[4]*Department of Physics and Astronomy, Vanderbilt University, Nashville, Tennessee, 37235, USA*
[5]*Department of Electrical Enginering, Princeton University, Princeton, New Jersey 08544, USA*
(Received 21 January 2004; published 2 September 2004)

We have studied the growth of pentacene films (2–8 monolayers) on modified Si-wafer surfaces by means of synchrotron x-ray diffraction. The diffraction data reveal a nonthermal damping of the (coherent) Bragg reflection intensities according to an exponential dependence on the $3/2$ power of the momentum transfer. The simultaneous presence of strong diffuse scattering centered around the Bragg positions indicates the presence of local defects. A quantitative analysis of the Bragg and diffuse scattering allows us to identify screw and edge dislocations as the main defects on the molecular scale. We quantify dislocation densities as a function of substrate termination.

DOI: 10.1103/PhysRevB.70.125401 PACS number(s): 68.35.Rh, 68.55.Nq

I. INTRODUCTION

Small organic conjugated molecules are currently the subject of intense research due to their large potential for organic and molecular electronics. Among the various materials under investigation, pentacene ($C_{22}H_{14}$), a long, flat, aromatic molecule [Fig. 1(a)] is particularly promising, since it easily forms layered crystals [Fig. 1(b)] if deposited onto flat, inert surfaces, resulting in highly anisotropic transport properties.[1] Pentacene may be used to fabricate organic thin film transistors (OTFT's) in applications where large area coverage, flexibility, and room temperature deposition processes are required.[2,3] In such devices, high-field mobilities on the order of 1.5 $cm^2/(V\,s)$ (Refs. 4 and 5) have been reported.

Extensive work has been dedicated to characterize the morphology of thin pentacene films (10 nm to 1 μm) on various substrates such as SiO_2,[7,8] Si,[9] Ag,[10] H-terminated Si,[7] passivated Si,[11] and polymer surfaces.[12] In these studies, surface modification, the growth temperature, flux, and kinetic energy of the deposited molecules[10] were all varied to study their influence on the apparent grain/island sizes, their roughness, and the orientation of the molecular axis (lying down versus standing up). These studies show the extent to which traditional growth concepts such as diffusion-limited aggregation[13–16] (applicable to a large class of inorganic heteroepitaxy systems) can be adapted for organic systems.[8,11,12,17] Another motivation for these structural studies is to understand and optimize the performance of pentacene devices by correlating electronic and structural properties.[1–5,18–25]

It is now established that grain boundaries in OTFT's [Fig. 1(c)] may act as traps for charge carriers.[26–28] But little is known about the degree of disorder at the molecular level of thin film devices (vacancies, dislocation types and densities, small angle boundaries, etc.). Recent high-resolution transmission electron microscopy (HRTEM) studies of edge-on pentacene crystallites nucleated on friction-transferred polymer substrates show that dislocations are present,[29] suggesting that this may be the case for other substrates, too. It is well known that structural defects have a strong influence on the charge transport of inorganic semiconductors; therefore the dislocation density may act as a benchmark for the quality of crystalline materials and in turn, device performance. Moreover, first principles calculations indicate that the details of the molecular arrangements may also have an influence on the transport properties of organic crystals.[30]

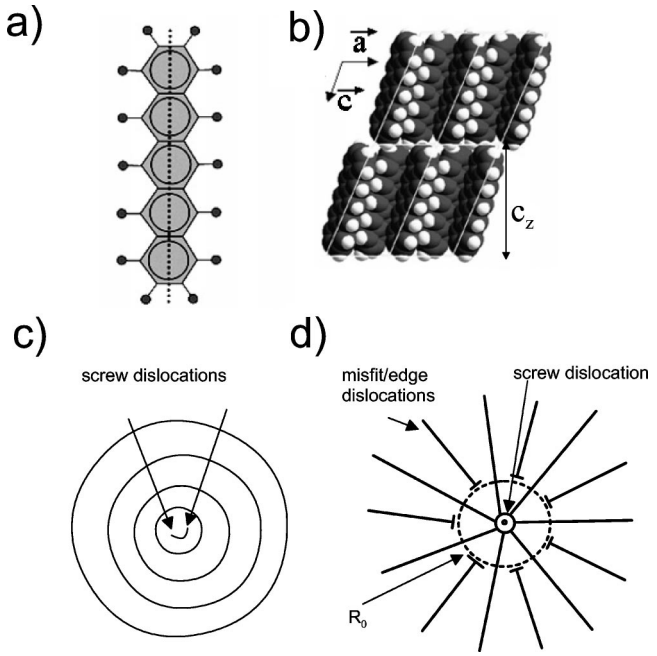

FIG. 1. (a) Pentacene ($C_{22}H_{14}$) molecule. (b) Side view of the layered structure of pentacene. (c) Pyramidal growth assisted by screw dislocations with opposite sign. The solid lines indicate molecular steps (1.5 nm). (d) Typical edge dislocation arrangement around a screw dislocation. This dislocation arrangement is equivalent to splay-bend (and sometimes bend-twist) disclination (Ref. 6).

Here, we report a synchrotron x-ray diffraction experiment that addresses structural defect densities in pentacene films by measuring the Bragg intensity dependence on momentum transfer and large sections of reciprocal space around the Bragg reflections, thus revealing diffuse scattering related to defects.

II. DISLOCATIONS, DISTORTIONS, AND MORPHOLOGY

In molecular beam epitaxy, the substrate temperature and the rate of deposition determine crucial film parameters such as island/grain size distribution, crystallinity and roughness.[31] In the low flux regime, molecules diffuse along the surface and a layer-by-layer growth is possible. However, in this growth mode, new nuclei have to form after the closure of each layer. Thus, layer-by-layer growth is not continuous. Therefore, initial layer-by-layer growth tends to convert into a much faster, defect-assisted growth mode. A prominent example is screw-dislocation-assisted growth, manifesting itself in the simplest scenarios by spiral growth patterns.[32] Often, pairs of screw dislocations, with opposite sign (Frank-Read source[33]), are energetically more stable, giving rise to more complex growth patterns such as pyramidal or conical, staircaselike growth as shown in Fig. 1(c) where the lines indicate molecular steps.[34] Usually, screw dislocations are accompanied by edge dislocations to adjust the different splaying "branches,"[35] as shown schematically in Fig. 1(d). For clarity, only one screw dislocation is shown.

Dislocations give rise to distortion fields. Molecules can be displaced in their entirety along the chain axes or in the transverse direction. If the substrate is flat and rigid, it constrains these movements considerably. Further peculiarities of distortion fields in pentacene arise from the weak H-H interactions between cleaving planes (*a*-*b* plane), leading to a crystalline film exhibiting much stronger lateral interactions than along the surface normal.[36] This implies a highly anisotropic response to external forces, favoring distortions along the surface normal. Therefore, we will assume that the dominant defects are screw dislocations with a Burgers vector **b** along the long axis of the pentacene molecules.

The screw dislocations are accompanied by a network of misfit (edge) dislocations, as shown in Fig. 1(d). The ends of the edge dislocations form prismatic loops with radius R. One screw dislocation may be surrounded by many loops of different radius. In our simplified model, we take this into account by introducing a density n_L defined as the loops per unit volume, and by introducing an average loop radius R_0. n_L may be converted to an areal density by multiplication with the film thickness D. n_L (by definition) represents an upper estimate of the number of screw dislocations.

The straight dislocation density per unit area (screw and edge dislocations) is denoted as n. n is related to n_L and R_0 by[37] $3n_L R_0 = n$. Equivalently,

$$R_0 = \sqrt{[n_L R_0^3]3/[n]}. \tag{1}$$

III. SCATTERING THEORY

A quantitative analysis of disorder at the molecular scale throughout the film is possible by means of x-ray diffraction experiments. The scattering intensity of a defective layer can be written within the kinematic approximation as follows:

$$I(\mathbf{q}) = I_B(\mathbf{q}) + I_D(\mathbf{q}). \tag{2}$$

Here I_B describes the coherent (Bragg) scattering, I_D is the diffuse scattering intensity, and $\mathbf{q}$ is the momentum transfer. Analyzing the diffuse and Bragg scattering, it is possible to quantify defect types and densities.

A. Bragg scattering

Let us define the reciprocal-lattice vector $\mathbf{k}_{HKL}$ corresponding to the average lattice of the crystalline pentacene film. In the following, we focus on reflections in the specular direction, i.e., k_{00L}. Then, $k_{00L} = L(2\pi/c_z)$, where L is the Miller index, and the thickness of a molecular layer is c_z, as shown in Fig. 1(b).

Displacements will contribute to a static, nonthermal Debye-Waller factor (DWF) damping of the initial Bragg intensities $I_B(k_{00L})$. The damped Bragg intensity is

$$I_B(q_z) = I_0(q_z)\exp(-2W). \tag{3}$$

Here, I_0 represents the diffracted intensity of the undistorted lattice and $\exp(-2W)$ describes the static damping. If strong static distortions dominate the DWF (i.e., $2W > 1$ and $\mathbf{q}\cdot\mathbf{b} \geqslant 1$, where $\mathbf{b}$ is the Burgers vector), the leading term of the DWF may be expressed as

$$2W = n_L R_0^3 (\mathbf{q}\cdot\mathbf{b})^{3/2} f(\mathbf{m}). \tag{4}$$

Here, $\mathbf{m} = \mathbf{q}/q$ is the normalized scattering vector pointing along the direction of the momentum transfer $\mathbf{q}$ and $f(\mathbf{m})$ is a contrast factor of the order of one. The value of $f(\mathbf{m})$ depends only on the orientation of the diffraction vector with respect to the misfit dislocations. Thus, $f(\mathbf{m})$ exhibits no L dependence for $00L$ type reflections. Furthermore, if the Burgers vector $\mathbf{b}$ is along the long axis of the molecule [Fig. 1(d)], then Eq. (4) further simplifies to

$$2W \cong (2\pi)^{3/2} n_L R_0^3 L^{3/2} f(\mathbf{m}) = \Delta_B L^{3/2}. \tag{5}$$

In turn, the parameter $n_L R_0^3 f(\mathbf{m})$ can be determined from a plot of the logarithm of the Bragg intensities I_B versus $L^{3/2}$. Qualitatively, $n_L R_0^3 \approx 1$ implies that the whole film contains dislocations while $n_L R_0^3 \ll 1$ implies that the defective areas are in coexistence with rather large, undistorted regions.

B. Diffuse scattering

Due to the presence of misfit dislocations and dislocation loops, the reciprocal-lattice points of the real pentacene crystal are misoriented and displaced relative to the ideal lattice. Relative to each reciprocal-lattice point we introduce the reduced momentum transfer $\boldsymbol{\tau} = (\mathbf{q} - \mathbf{k}_{00L})/k_{00L}$. Here, $\mathbf{q}$ is located in the vicinity of the Bragg position. Experimentally, $\boldsymbol{\tau}$ is chosen by changing the angle of incidence (Θ) while keeping the scattering (detector) angle 2Θ constant. $\boldsymbol{\tau}$ is also called the misorientation vector and the corresponding scan is called a rocking scan [see Fig. 2(a)]. The diffuse intensity around each reciprocal-lattice point is a function of the mis-

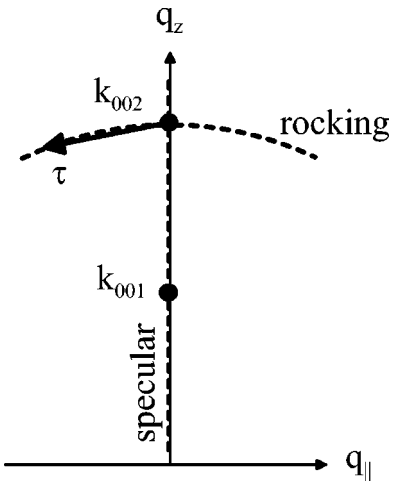

FIG. 2. Diffraction geometry. Reciprocal-space scheme indicating the directions of specular and rocking scan. Also shown are the k_{00L} positions and the misorientation vector τ.

orientation vector $\boldsymbol{\tau}$. For the calculation of the rocking curve, we average the intensity distribution in the plane perpendicular to the rocking axis to account for the anisotropic resolution element in this geometry.

A linear increase of the full width at half maximum of the diffuse intensity $\kappa_{\|}^{D}$ with k_{00L} is characteristic of defects associated with nonuniform strain fields, as found also in simple models of misfit dislocations at the interface of inorganic films.[38,39] For pentacene, assuming equal density of misfit dislocations for all slip systems, we obtain a linear dependence on the dislocations density n and on the layer thickness c_z. This is typical for strain gradient fields due to unpaired dislocations[40]

$$\kappa_{\|}^{D} = 10nc_z k_{00L} bC(\mathbf{m},\mathbf{b}). \tag{6}$$

Here, $C(\mathbf{m},\mathbf{b})$ is an orientation-dependent contrast factor $C \sim 1$. Assuming $b=c$, Eq. (6) simplifies to

$$\kappa_{\|}^{D} \cong 20\pi c_z nLC(\mathbf{m},\mathbf{b}) = \Delta_D L. \tag{7}$$

Thus, the straight dislocations density per unit area n can be estimated from a linear plot of the diffuse (rocking scan) intensity width $\kappa_{\|}^{D}$ versus the Miller index L, if some assumptions about $C(\mathbf{m},\mathbf{b})$ are made. Typically, the contrast factors $f(\mathbf{m})$ and $C(\mathbf{m},\mathbf{b})$ are of the order of unity. The detailed analysis of contrast factors is possible only if Bragg reflections in different directions are studied. In the experimental work presented below, we focus on Bragg reflections along the surface normal. Hence, $f(\mathbf{m})$ and $C(\mathbf{m},b)$ are set to 1 in the analysis. In order to extract the average radius of dislocation loops R_0, one may make use of the relation (1).

IV. EXPERIMENTAL DETAILS

Since pentacene film formation is controlled by relatively weak van der Waals interactions, nucleation of the first monolayer (ML) is extremely sensitive to the presence of defects or impurities on the substrate surface, which act as

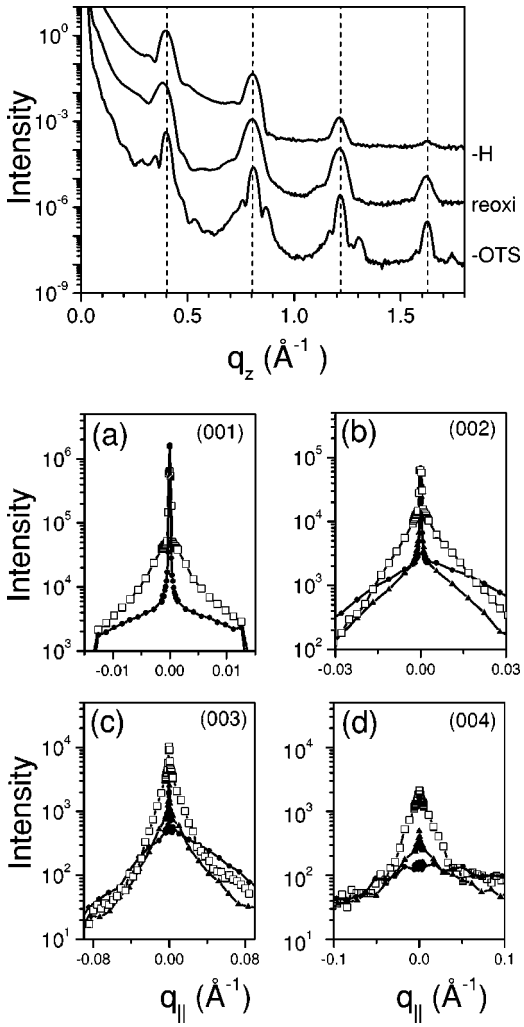

FIG. 3. X-ray intensities for a nominal coverage of 8 ML. Top panel: Reflectivity data recorded under specular conditions for different surface terminations (from top to bottom: H terminated, reoxidized, OTS-grafted surface). Bottom panels (a–d): X-ray rocking scan intensities. The scans are performed at the center of the 00L Bragg reflections (dashed lines in the top panel of Fig. 3). (a) $L=1$ (b) $L=2$, (c) $L=3$ (d) $L=4$. The OTS, H termination, and reoxidized surface are indicated by squares, disks, and triangles, respectively.

pinning centers. To minimize the influence of surface impurities, we applied a three-step wet-etching procedure to silicon (100) wafers with a 10 nm thermally grown oxide.[7] Step I removes organic contamination at the thermal oxide surface. During step II, the thermal oxide is removed, and after rinsing, the surface becomes H terminated. Step III is intended to reoxidize the topmost Si bilayer in a controlled way. For comparison, pentacene was also deposited on an octadecyltrichlorosilane (OTS) layer grafted to a thermal oxide (100 Å) following a procedure described in Ref. 3.

Pentacene films were evaporated *in situ* in a transportable vacuum chamber equipped with a 270° beryllium window, a Knudsen cell, a quartz crystal microbalance, and a sample holder that allows temperature control in the range of 200–500 K. The deposition rate was kept at 1.25×10^{-3}nm/sec (or 1 ML/20 min assuming 1 ML is 1.5 nm)

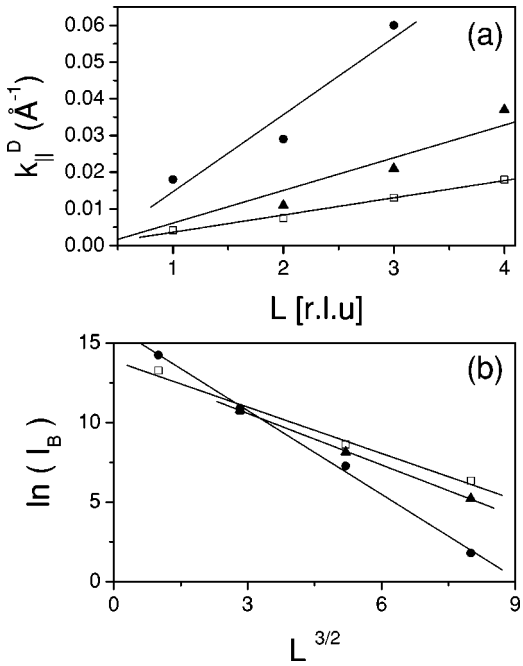

FIG. 4. X-ray analysis. (a) The full width half maximum of the diffuse intensity $\kappa_{||}^{D}$ is plotted versus L. The Miller index is reported in reduced lattice units. (b) The logarithm of the Bragg intensity $[\ln(I_B)]$ is plotted versus the scaled momentum transfer $(L^{3/2})$. The OTS, H termination, and reoxidized surface are indicated by squares, disks, and triangles, respectively, in both plots.

for all experiments with the substrate held at room temperature during deposition. The background pressure during evaporation was 1×10^{-7} Torr.

X-ray experiments were carried out at the National Synchrotron Light Source (NSLS) at the Exxon beamline X10b. The wavelength was fixed at 0.1123 nm. Pentacene films were evaporated on H-terminated, on reoxidized, and on OTS-terminated wafers. The duration between surface preparation and evacuation of the sample environment was less than 30 min.

The layered pentacene structure gives rise to Bragg peaks at the $k_{00L}=L2\pi/c_z$ positions, as indicated in Fig. 2. Specular scans determine the layer thickness c_z [see Fig. 1(b)]. At selected q_z positions, rocking scans divide the intensity distribution into a resolution-limited, delta-shaped Bragg component and broad diffuse scattering.

V. RESULTS

The specular intensities of all pentacene films are summarized in the top panel of Fig. 3. The curves have been displaced vertically for clarity. The reflectivity behavior towards smaller q is superimposed on a series of Bragg reflections induced by the layered structure of the films. The vertical dashed lines indicate the Bragg positions for a lattice spacing of $c_z=15.5$ Å. This lattice spacing is characteristic for the "thin-film phase" of pentacene on inert surfaces for room temperature deposition. Depending on the growth parameters, other phases may also be present. Bulk phase pentacene, for example, exhibits a lattice spacing of $c_z=14.4$ Å.[41]

The finite peak width along q_z, $\Delta q_z=0.048$ Å^{-1} for the H-terminated surface and $\Delta q_z=0.055$ Å^{-1} for the reoxidized surface, can be converted to a thickness D using the relation $D=2\pi/\Delta q_z$. $D=130$ Å is obtained for the H-terminated surface and $D=114$ Å for the reoxidized surface. Both numbers agree with the nominal film thickness of $D=8$ ML $\times 15.5$ Å$=124$ Å, given that the evaporation rate is only accurate to about 10% and that the sticking coefficient may differ from unity. The OTS-templated film, however, exhibits a much narrower linewidth ($\Delta q_z=0.029$ Å^{-1} or $D=216$ Å). Additionally, the peak splitting is clear evidence of the presence of two structurally different phases: a dominant "thin film" phase ($c_z=15.5$ Å, vertical dashed lines in the top panel of Fig. 3) and some degree of bulk phase pentacene (14.4 Å). Thus, growth on OTS is more heterogeneous.

In order to further characterize the origin of the diffracted intensities, rocking scans were performed at the center of the Bragg reflections. The results are summarized in Figs. 3(a)–3(d). The scans reveal a sharp and a broad component, both with a pronounced L dependence.

The sharp component may be identified as the resolution-limited Bragg signal from the average lattice I_B. With increasing L, I_B is strongly damped, as expected for the presence of static disorder [Eq. (3)]. The damping of the Bragg intensity with L is analyzed by plotting the logarithm of the Bragg intensity $[\ln(I_B)]$ versus the scaled momentum transfer $(L^{3/2})$ [Fig. 4(b)]. In agreement with Eq. (5), a linear behav-

TABLE I. Summary of the parameters determined from the linear regressions in Fig. 4. The surface termination of the substrate is indicated in the first column. The negative slope Δ_B of the Bragg intensity as function of $L^{2/3}$ is reported in the second column, and, using Eq. (5), these numbers are converted to $n_L R_0^3$ (third column). The slope Δ_D of the increase of the diffuse intensity width $\kappa_{||}^{D}$ with L is reported in the fourth column, and, using Eq. (7), these numbers are converted to the straight dislocation density per unit area n, and reported in the fifth column. The estimate of the average radius of dislocation loops R_0, based on Eq. (1), is reported in column 6. The areal loop density, obtained from $n_L R_0^3$ (col. 3), R_0 (col. 6), and a film thickness $D\simeq 120$ Å, is reported in the last column.

Surface	Δ_B	$n_L R_0^3$	Δ_D (10^{-3} Å^{-1})	n (10^{11} cm^{-2})	R_0 (Å)	$n_L D$ (10^{11} cm^{-2})
H terminated	1.75±.06	0.11±.003	21±5	2.1±.5	125±30	0.67
Reoxidized	1.08±.02	0.07±.001	8.8±1.6	0.9±.2	153±30	0.24
OTS	0.97±.08	0.06±.005	4.7±0.3	0.5±.03	190±20	0.11

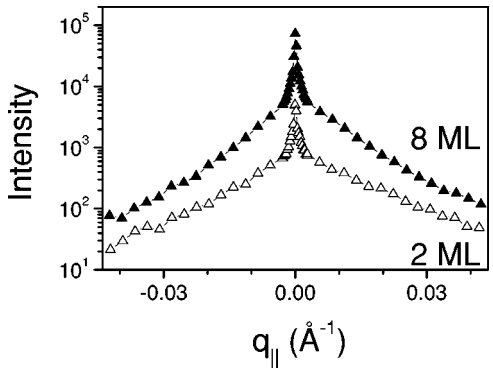

FIG. 5. Thickness dependence. The (002) rocking scan of a 2 ML and a 8 ML pentacene film deposited on piranha-cleaned thermal silicon oxide.

ior is found [solid lines in Fig. 4(b)]. The slopes Δ_B and the parameter $n_L R_0^3$ [using Eq. (5) and assuming $f(m)=1$] are summarized in Table I.

The broad component in Figs. 3(a)–3(d) represents diffuse scattering I_D. The scaling of the $\kappa_{\|}^D$ width of the diffuse intensity with L [Eq. (6)] is determined by the full width at half maximum (FWHM) of the diffuse scattering intensity [Fig. 3(a)–3(d)]. The L dependence of the respective width is summarized in Fig. 4(a). The linear slope Δ_D is determined from a linear regression [solid lines in Fig. 4(a)] and the slope is converted to n using Eq. (7). The numbers are summarized in Table I. The estimates of R_0, based on Eq. (1), are summarized in column 6 of Table I.

The dependence of the diffuse intensities on film thickness was studied by comparing the scattering from a 2 ML and an 8 ML pentacene film deposited on (piranha-cleaned[7]) (Step I) thermal silicon oxide. The data are depicted in Fig. 5. Apparently, the overall intensity increases with coverage, while the line shape hardly changes. This indicates that defects forming at the initial stage of growth propagate throughout the film and, in turn, the (areal) dislocation density n is constant with thickness.

In order to verify that the diffuse scattering originates from static distortion rather than thermal disorder, a control experiment at 130 K (using a closed cycle refrigerator) was performed in the vicinity of the (003) reflection. Hardly any change is observed in the diffuse or in the Bragg scattering, confirming the static character of the distortions, which are responsible for the damping of the Bragg intensities and the generation of diffuse scattering.

VI. DISCUSSION

For an OTS-terminated silicon wafer, a 1 cm^2 pentacene patch contains about $n=0.5\times10^{11}$ dislocations (see Table I). The same patch on a silicon oxide surface has about $n=0.9\times10^{11}$ dislocations, while on H-terminated silicon, the dislocation density is as high as $n=2.1\times10^{11}/cm^2$. Thus, all films exhibit significant dislocation densities, with the H-terminated surface resulting in the highest density.

The (independent) analysis of the damping of the Bragg component with increasing momentum transfer L confirms this ranking, with the static damping being largest for the H-terminated surface, lowest for OTS termination, and in between for the reoxidized surface. The effective radius of dislocation loops R_0 is microscopic in all cases. For the H-terminated surface, R_0 is 125 Å, while it is 153 and 190 Å for the reoxidized and OTS-terminated surface, respectively. This implies that dislocations emerge close to the center of a screw dislocation.

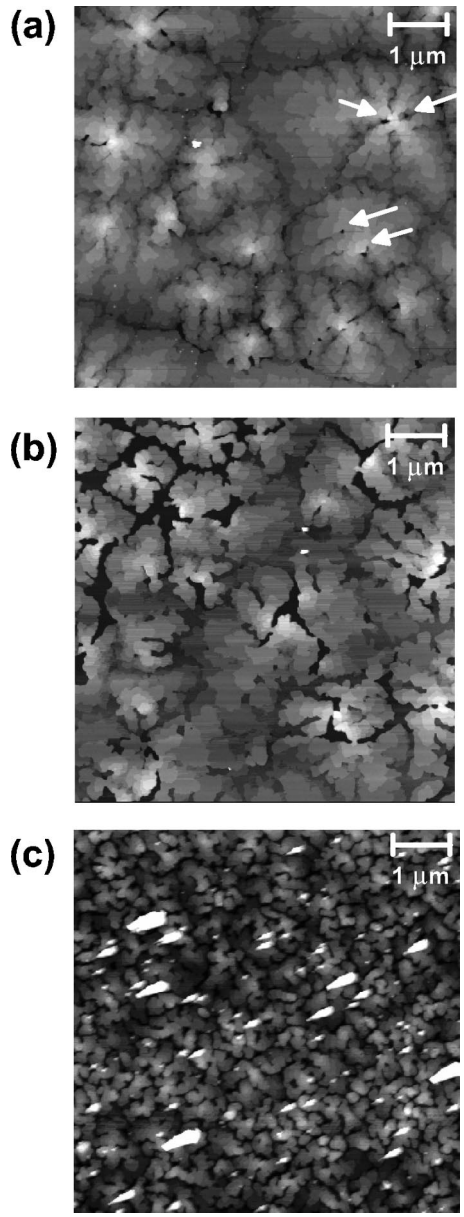

FIG. 6. AFM micrograph (7.5 μm$\times$7.5 μm). The gray scale represents relative height and ranges from black (zero height) to white (height given below): (a) H terminated (30 nm), (b) reoxidized (25 nm),(c) OTS-terminated (35 nm).

Atomic force microscopy (AFM) micrographs of the nominally 8 ML films have been obtained *ex situ* in tapping mode (Fig. 6) after completing the x-ray study. For the H-terminated Si surface [Fig. 6(a)], the apparent grain size is several μm. Close inspection reveals the presence of deep holes, which are often located close to the center/top of the

grains. Almost all of these deep holes represent an end point of canyonlike valleys. For clarity, some of these holes are marked by white arrows. We suggest that these holes are "hollow cores," i.e., screw dislocations with an empty core. Hollow cores are possible if the energy to create the free surface of the empty core is compensated by avoiding the buildup of stress energy in the center of a screw dislocation. It was predicted by Franck[42] that these defects are possible in organic materials such as protein crystals if the long axis of the unit cell exceeds 10 Å. Recently, hollow cores were also found in organic thin films of radical *p*-nitrophenyl nitroxyl nitroxide (*p*-NPNN).[43,44]

For the reoxidized Si surface [Fig. 6(b)], the grain size is reduced to about 1 μm diameter. Some deep holes close to the top of the islands are still visible.

On the OTS layer the pentacene grain size is further reduced to the submicron region [Fig. 6(c)], and no "hollow cores" are observed, and the films exhibit the lowest density of straight dislocations n (Table I). Remarkably, pentacene films grown on OTS exhibit a carrier mobility larger than films grown on clean oxide.[3] We suggest that this might be due to the reduced amount of straight dislocations.

It is also illuminating to compare the areal densities determined from the x-ray analysis (Table I, columns 5 and 7) of the AFM micrographs. For example, the film grown on the H-terminated surface exhibits an areal loop density of 0.67×10^{11} cm^2 (or 670 μm^2), and an areal dislocation density of 2100 μm^{-2}. A micrometer patch of the same film [Fig. 6(a)] shows only about one pair of hollow cores, indicating that the number of loops per screw dislocation is very large.

Pentacene grown on OTS exhibits the highest nucleation density, the lowest dislocation density, and the coexistence of the pentacene thin film phase with a three-dimensional growth mode. One may speculate that enhanced supersaturation (if compared to the more inert oxide and H-terminated surface) is the physical origin of these effects.

The large damping of Bragg intensities reported in this study is present in most of the published literature on pentacene films,[1,45–47] indicating that a large defect density is a general phenomenon in pentacene thin films, rather than one specific to the growth conditions chosen in this work. The presence of diffuse scattering requires verification by rocking scans over a large angular range. An inverse proportionality between rocking scan width for organic films and their electrical mobilities was reported recently.[48] Our analysis indicates that diffuse scattering and Bragg scattering must be disentangled in order to draw conclusions about the microscopic nature of the film.

VII. SUMMARY

In summary, we have quantified dislocation densities in pentacene thin films from the static damping of Bragg intensities and from the width of diffuse scattering intensities. Our analysis shows that defect densities are very high in pentacene films. This should be taken into account for a molecular understanding of transport properties in organic films and for the comparison of transport in thin films and highly perfect single crystals. A detailed description of the diffuse intensity line shape should reveal the local distortions around defects in detail. For this, however, future experiments should be extended to nonspecular Bragg peaks.

ACKNOWLEDGMENTS

We thank the NSLS management and the beamline staff and scientists from Exxon (Steven Bennett and Rainer Kolb) for continuous support and Ben Ocko for providing access to a closed cycle refrigerator. Max Shtein from the Princeton University Electrical Engineering is acknowledged for help with the preparation of the OTS termination. Fatih Danisman from the Princeton University Chemistry Department is acknowledged for help with organizing the synchrotron experiments. The work at Princeton and at the NSLS was supported by the DOE under Grant No. DE-FG02-93ER45503 and by the NSF (DMR-0097133). B.N. acknowledges support from the Deutsche Forschungsgemeinschaft (DFG Ni632/1-1). R.B. acknowledges the support of the Director, Office of Science, Office of Basic Energy Sciences, U.S. Department of Energy, under Contract No. DE-AC05-00OR22725 with UT-Battelle.

*Present address: Ludwig-Maximilians-Universität München, Germany. Electronic address: bert.nickel@physik.uni-muenchen.de

†Electronic address: barabashr@ornl.gov

‡Present address: Cornell University, Cornell Center for Materials Research, Ithaca, NY 14853.

[1] T. Minakata, H. Imai, M. Ozaki, and K. Saco, J. Appl. Phys. **72**, 5220 (1992).

[2] D. Knipp, R. A. Street, B. Krusor, R. Apte, and J. Ho, J. Non-Cryst. Solids **299**, 1042 (2002), part B.

[3] M. Shtein, J. Mapel, J. B. Benziger, and S. R. Forrest, Appl. Phys. Lett. **81**, 268 (2002).

[4] Y. Y. Lin, D. J. Gundlach, S. F. Nelson, and T. N. Jackson, IEEE Electron Device Lett. **18**, 606 (1997).

[5] Y. Y. Lin, D. J. Gundlach, S. F. Nelson, and T. N. Jackson, IEEE Trans. Electron Devices **44**, 1325 (1997).

[6] F. R. N. Nabarro, in *Dislocations in Solids*, edited by H. Suzuki, T. Ninomiya, K. Simino, and S. Takeuchi (VSP, Zeist, The Netherlands, 1985).

[7] R. Ruiz, B. Nickel, N. Koch, L. Feldman, R. Haglund, A. Kahn, and G. Scoles, Phys. Rev. B **67**, 125406 (2003).

[8] R. Ruiz, B. Nickel, N. Koch, L. C. Feldman, R. F. Haglund, A. Kahn, F. Family, and G. Scoles, Phys. Rev. Lett. **91**, 136102 (2003).

[9] M. Kasaya, H. Tabata, and T. Kawai, Surf. Sci. **406**, 302 (1998).

[10] L. Casalis, M. F. Danisman, B. Nickel, G. Bracco, T. Toccoli, S. Iannotta, and G. Scoles, Phys. Rev. Lett. **90**, 206101 (2003).

[11] F.-J. Meyer Zu Heringdorf, M. C. Reuter, and R. M. Tromp, Nature (London) **412**, 517 (2001).

[12] Y. Luo, G. H. Wang, J. A. Theobald, and P. H. Beton, Surf. Sci. **537**, 241 (2003).
[13] T. A. Witten, Jr. and L. M. Sander, Phys. Rev. Lett. **47**, 1400 (1981).
[14] F. Family and P. Meakin, Phys. Rev. Lett. **61**, 428 (1988).
[15] J. G. Amar, F. Family, and P.-M. Lam, Phys. Rev. B **50**, 8781 (1994).
[16] J. G. Amar and F. Family, Phys. Rev. Lett. **74**, 2066 (1995).
[17] F. Biscarini, P. Samori, O. Greco, and R. Zamboni, Phys. Rev. Lett. **78**, 2389 (1997).
[18] D. J. Gundlach, Y. Lin, T. Jackson, S. Nelson, and D. Schlom, IEEE Electron Device Lett. **18**, 87 (1997).
[19] C. R. Kagan, D. B. Mitzi, and C. D. Dimitrakopoulos, Science **286**, 945 (1999).
[20] H. Klauk and T. N. Jackson, Solid State Technol. **43**, 63 (2000).
[21] D. J. Gundlach, L. L. Jia, and T. N. Jackson, IEEE Electron Device Lett. **22**, 571 (2001).
[22] C. D. Dimitrakopoulos and P. R. L. Malenfant, Adv. Mater. (Weinheim, Ger.) **14**, 99 (2002).
[23] V. Y. Butko, X. Chi, D. V. Lang, and A. P. Ramirez, Appl. Phys. Lett. **83**, 4773 (2003).
[24] D. V. Lang, X. Chi, A. M. Sergent, and A. P. Ramirez, cond-mat/0312721 (unpublished).
[25] D. V. Lang, X. Chi, T. Siegrist, A. M. Sergent, and A. P. Ramirez, cond-mat/0312722 (unpublished).
[26] G. Horowitz and M. E. Hajlaoui, Adv. Mater. (Weinheim, Ger.) **12**, 1046 (2000).
[27] G. Horowitz and M. E. Hajlaoui, Synth. Met. **122**, 185 (2001).
[28] G. Horowitz and M. E. Hajlaoui, Synth. Met. **121**, 1349 (2001).
[29] M. Brinkmann, S. Graaf, C. Straup, J.-C. Wittmann, C. Chaumont, F. Nuesch, A. Aziz, M. Schaer, and L. Zuppiroli, J. Phys. Chem. B **107**, 10531 (2003).
[30] J. L. Bredas and S. Marder, Adv. Funct. Mater. **12**, 555 (2002).
[31] J. A. Venables, G. D. T. Spiller, and M. Hanbrcken, Rep. Prog. Phys. **47**, 339 (1984).
[32] S. Amelinckx, Nature (London) **167**, 939 (1951).
[33] F. C. Frank and W. T. Read, Phys. Rev. **79**, 722 (1950).
[34] R. F. Xiao, J. I. D. Alexander, and F. Rosenberger, Phys. Rev. A **43**, 2977 (1991).
[35] P. Cladis and M. Kleman, J. Phys. (France) **33**, 591 (1972).
[36] J. E. Northrup, M. L. Tiago, and S. G. Louie, Phys. Rev. B **66**, 121404 (2002).
[37] M. Krivoglaz, *Diffuse Scattering of X-Rays and Neutrons by Fluctuations*, edited by S. Moss, J. Peisl, V. Baryakhtar, and M. Ivanov (Springer, Berlin, 1996).
[38] V. M. Kaganer, R. Kohler, M. Schmidbauer, R. Opitz, and B. Jenichen, Phys. Rev. B **55**, 1793 (1997).
[39] R. I. Barabash, W. Donner, and H. Dosch, Appl. Phys. Lett. **78**, 443 (2001).
[40] R. Barabash, G. E. Ice, B. C. Larson, G. M. Pharr, K. S. Chung, and W. Yang, Appl. Phys. Lett. **79**, 749 (2001).
[41] R. B. Campbell, J. M. Robertson, and J. Trotter, Acta Crystallogr. **14**, 705 (1961); **15**, 289 (1962).
[42] F. Frank, Acta Crystallogr. **415**, 497 (1951).
[43] J. Fraxedas, J. Caro, A. Figueras, P. Gorostiza, and F. Sanz, Surf. Sci. **415**, 241 (1998).
[44] J. Fraxedas, J. Caro, J. Santiso, A. Figueras, P. Gorostiza, and F. Sanz, Phys. Status Solidi B **215**, 859 (1999).
[45] H. Akimichi, T. Inoshita, S. Hotta, H. Noge, and H. Sakaki, Appl. Phys. Lett. **63**, 3158 (1993).
[46] C. D. Dimitrakopoulos, A. R. Brown, and A. Pomp, Appl. Phys. Lett. **80**, 2501 (1996).
[47] D. J. Gundlach, T. N. Jackson, D. G. Schlom, and S. F. Nelson, Appl. Phys. Lett. **74**, 3302 (1999).
[48] N. Karl, Synth. Met. **133**, 649 (2003), sp. Iss. SI.